Revealing the Complex Nature of Bonding in the Binary High-Pressure Compound FeO 2

E. Koemets, I. Leonov, M. Bykov, E. Bykova, S. Chariton, G. Aprilis, T. Fedotenko, S. Clément, J. Rouquette, Julien Haines, et al.

Revealing the Complex Nature of Bonding in the Binary High-Pressure Compound FeO_2

E. Koemets,[1,2,*] I. Leonov,[3,4,5,†] M. Bykov,[1] E. Bykova,[1,6] S. Chariton,[1] G. Aprilis,[7,8] T. Fedotenko,[7] S. Clément,[9] J. Rouquette,[2] J. Haines,[2] V. Cerantola,[8] K. Glazyrin,[10] C. McCammon,[1] V. B. Prakapenka,[11] M. Hanfland,[8] H.-P. Liermann,[10] V. Svitlyk,[8] R. Torchio,[8] A. D. Rosa,[8] T. Irifune,[12] A. V. Ponomareva,[4] I. A. Abrikosov,[13] N. Dubrovinskaia,[7,13] and L. Dubrovinsky[1]

[1]*Bayerisches Geoinstitut, University of Bayreuth, D-95440 Bayreuth, Germany*
[2]*Institut Charles Gerhardt Montpellier (UMR CNRS 5253), Université de Montpellier, F-34095 Montpellier Cedex 5, France*
[3]*Institute of Metal Physics, Sofia Kovalevskaya Street 18, 620219 Yekaterinburg GSP-170, Russia*
[4]*Materials Modeling and Development Laboratory, NUST "MISIS", 119049 Moscow, Russia*
[5]*Ural Federal University, 620002 Yekaterinburg, Russia*
[6]*Carnegie Institution of Washington, Earth and Planets Laboratory, 5241 Broad Branch Road NW, Washington, DC 20015, USA*
[7]*Material Physics and Technology at Extreme Conditions, Laboratory of Crystallography, Universität Bayreuth, D-95440 Bayreuth, Germany*
[8]*The European Synchrotron Radiation Facility, 38043 Grenoble Cedex 9, France*
[9]*Laboratoire Charles Coulomb (L2C)—UMR CNRS 5221, Université de Montpellier, CC069, 34095 Montpellier, France*
[10]*Photon Science, Deutsches Elektronen-Synchrotron, D-22607 Hamburg, Germany*
[11]*Center for Advanced Radiation Sources, University of Chicago, Chicago, Illinois 60437, USA*
[12]*Geodynamics Research Center, Ehime University, 2-5 Bunkyo-cho, Matsuyama 790-8577, Japan*
[13]*Department of Physics, Chemistry and Biology (IFM), Linköping University, SE-581 83 Linköping, Sweden*

(Received 20 October 2020; revised 7 December 2020; accepted 7 January 2021; published 12 March 2021)

Extreme pressures and temperatures are known to drastically affect the chemistry of iron oxides, resulting in numerous compounds forming homologous series $n\mathrm{FeO}m\mathrm{Fe_2O_3}$ and the appearance of FeO_2. Here, based on the results of *in situ* single-crystal x-ray diffraction, Mössbauer spectroscopy, x-ray absorption spectroscopy, and density-functional theory + dynamical mean-field theory calculations, we demonstrate that iron in high-pressure cubic FeO_2 and isostructural $FeO_2H_{0.5}$ is ferric (Fe^{3+}), and oxygen has a formal valence less than 2. Reduction of oxygen valence from 2, common for oxides, down to 1.5 can be explained by a formation of a localized hole at oxygen sites.

DOI: 10.1103/PhysRevLett.126.106001

At ambient (or low) pressures, three different iron oxides are known: Fe_2O_3 with a mineral name hematite; Fe_3O_4 magnetite—the oldest known magnetic material—and FeO wüstite, which is nonstoichiometric and typically iron deficient. At extreme pressures and temperatures, the synthesis yields numerous iron oxides with unexpected compositions (such as Fe_4O_5, Fe_5O_6, Fe_7O_9, Fe_5O_7, $Fe_{25}O_{32}$, etc.), unusual crystal structures, and intriguing physical properties, demonstrating the complexity of the binary Fe—O system [1–5]. It was suggested that iron oxides at high-pressure and high-temperature conditions (HP-HT) could be systematized by homologous structural series $n\mathrm{FeO}m\mathrm{Fe_2O_3}$ formed by oxygen (O^{2-}) and iron in ferrous and/or ferric states (Fe^{2+} and Fe^{3+}, correspondingly). Besides the end members, iron could exist in the mixed-valence state in this series (formally intermediate between 2+ and 3+ valence), defined by the stoichiometry of HP iron oxides. However, the recent finding of cubic FeO_2 (space group $Pa\bar{3}$), and closely related FeO_2H_x (x up to 1) phases [6–8], suggests that not only iron but also oxygen could have a variable oxidation state in iron oxides (or oxyhydroxides).

Powder x-ray diffraction (PXRD) [6], x-ray absorption spectroscopy (XAS) [9,10], and nuclear forward scattering (NFS) studies [10] of cubic high-pressure FeO_2H_x ($x = 0$–1) compounds, as well as results of some theoretical works [11,12] were used to argue that iron is ferrous in these phases even at strongly oxidized conditions and thus oxygen forms peroxide $(O_2)^{2-}$ ions. However, the question concerning the oxidation state of both iron and oxygen in FeO_2 and FeO_2H_x remains controversial, primarily because of harsh experimental conditions and ambiguous results. For example, while XAS data were interpreted to indicate that iron is ferrous [9,10], NFS data of cubic FeO_2 [10] show center shifts (~0.15 mm/s at 80 GPa) that are unrealistic for any ferrous compound.

Available experimental information on the crystal structure of FeO_2 and FeO_2H_x phases is based on PXRD [6,8], which makes the analysis of the Fe—O and O—O distances unreliable compared to more complex yet more informative

structural refinements from single-crystal x-ray diffraction data (SC-XRD) [13]. Additionally, some theoretical works [14–17] suggest that iron is ferric in FeO_2, illustrating the necessity of performing high-accuracy experiments to establish the physical and chemical properties of this phase.

The goals of this Letter are to clarify the high-pressure crystal chemistry of cubic FeO_2 and FeO_2H_x phases and determine the oxidation state of iron and oxygen. These are not only of importance as a fundamental problem for HP-HT chemistry, but also highly relevant for geosciences [6]. In order to achieve the goals of our studies, we perform multimethod synchrotron-based experiments, including advanced *in situ* SC-XRD, x-ray absorption, and Mössbauer spectroscopy using laser-heated diamond anvil cells (see Supplemental Material [18], Table S1). We support our experimental results by the density-functional theory + dynamical mean-field theory (DFT + DMFT) calculations [35,36] of the electronic structure and magnetic and valence states of iron. An application of DFT + DMFT provides a nonperturbative treatment of (local) spin fluctuations allowing one to determine the electronic structure and magnetic and structural properties of paramagnetic correlated materials, e.g., near the Mott transition [35]. We perform a full structural optimization and compute the crystal structure parameters of paramagnetic FeO_2 under pressure within DFT + DMFT [37–43]. Our experimental and theoretical results suggest that iron in HP-PdF_2-type FeO_2 and FeO_2H_x is ferric $(3+)$. We show the absence of a molecular $(O_2)^{-3}$ bonding state in HP-PdF_2-type FeO_2, implying that the oxidation state of oxygen is equal to 1.5– due to oxygen-metal negative charge transfer. Such a charge transfer is expected to shorten the Fe—O distance and consequently reduce the volume of FeO_6 octahedra, which should cause both iron polyhedra and the entire structure to become highly incompressible.

Compression of iron in oxygen at ambient temperature to 25(1) GPa did not produce any chemical reaction, but laser heating of the sample at this pressure to ~1500(100) K led to the formation of Fe_2O_3 [space group $R\bar{3}c$, unit cell parameters $a = 4.91496(3)$ Å, $c = 13.2579(1)$ Å] (see Fig. S2 [18]), in agreement with literature data [44]. After further compression to 46(2) GPa, the laser heating of a sample was performed at ~1200(100) K. The XRD pattern of the temperature-quenched product drastically changed (see Fig. S2 [18]). The XRD analysis shows cubic FeO_2 with the space group $Pa\bar{3}$ and unit cell parameter $a = 4.4313(14)$ Å, which is close to the values reported for "pyrite-type" FeO_2 [6,16]. Iterative heating of the samples at different pressures resulted in the growth of microcrystals of cubic FeO_2 that enabled performing an *in situ* SC-XRD data collection with further structure solution and refinements. The SC-XRD data analysis revealed that FeO_2 has the HP-PdF_2-type structure (see Table S1 [18]) in a range of pressures from 36(1) to 73(2) GPa. The compressional behavior of this phase was studied in several experimental runs on compression and decompression, as described in Table S1 and results are presented in Fig. 1. In our experiments, we did not observe the cubic FeO_2 phase at pressures below ~30 GPa. The results on the crystal structure refinements from *in situ* SC-XRD datasets of the FeO_2, which have never been reported before, are summarized in Table S2 (see Fig. S1). Structural analysis suggests that the O—O dimer bond length varies from 2.213(7) to 2.104(15) Å within the pressure range from ~36 to 73 GPa (see Table S2). For peroxides (in molecular or crystalline forms), the distances between the closest oxygen atoms at ambient pressure are very characteristic—from about 1.2 to 1.5 Å [45] (e.g., in MgO_2 it is about 1.492 Å), and under compression these distances should not increase. In the case of FeO_2, such a large observed O—O distance suggests, from a crystal-chemical point of view, the absence of chemical bonding between oxygen atoms. Even in the case of the structural model of FeO_2 refined against powder XRD data (pyrite-type FeO_2 [6]), the shortest O—O bond is ~1.896 Å at 76 GPa, which is too large for peroxides.

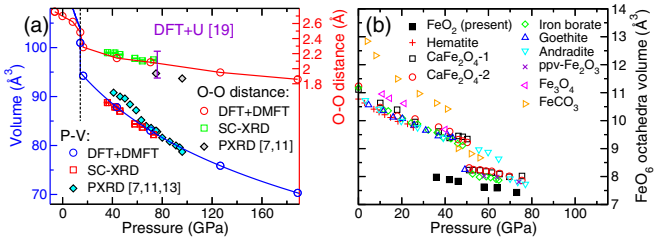

FIG. 1. Compressional behavior of HP-PdF_2-type FeO_2: (a) lattice volume and O—O distance obtained by DFT + DMFT at $T = 1160$ K in comparison to XRD data. DFT + DMFT predicts a spin-state transition at ~14 GPa, depicted by a dashed vertical line. (b) Pressure dependence of volumes of the FeO_6 octahedra in various compounds according to Ref. [46].

A number of transition metals, for example, osmium and ruthenium, the neighbors of iron in the VIIIb group of the periodic table, form dioxides, OsO_2 and RuO_2 with the HP-PdF_2-type structure [46,47] (space group $Pa\bar{3}$). The shortest O—O distance in these dioxides is equal to ~2.5 Å at ambient conditions. These phases are characterized by low compressibility (for details see Refs. [46,47]), and cubic FeO_2 is very incompressible as well, according to our experimental data [see Fig. 1(b)]. Accounting for the relatively long O—O distances in FeO_2 at HP, one could expect that it adopts rather the HP-PdF_2-type structure than forms a peroxide. Additionally, according to the "rule of thumb" [48], the behavior of compounds (particularly oxides) of an element at high pressure is similar to that of compounds of the elements with higher atomic number in the same group of the periodic table at low pressures.

The results of structural studies and crystal-chemical considerations are consistent and point toward highly unusual crystal chemistry of Fe—O bonds in

HP-PdF_2-type FeO_2. In fact, Streltsov *et al.* [14] suggested on the basis of *ab initio* calculations for FeO_2 that the valence of iron is 3+ and classified the material as lying "in between" oxides and peroxides with the anion described as $(O_2)^{3-}$. However, the structural model obtained from PXRD [6] was used in the calculations, and the input crystal structure of cubic FeO_2 was not optimized self-consistently [14]. While other electronic structure studies used the DFT + U method to compute the crystal structure parameters of FeO_2 [11,12,17], these computations assume the existence of a long-range magnetic order in HP-PdF_2 phase of FeO_2, in contradiction with experiment. As a result, such computations cannot give a reliable results for the shortest O—O bond length in FeO_2, predicting either an unusual increase of the O—O distance under pressure [11] or a large O—O distance of 2.232 Å at 76 GPa [17].

We resolve this point by computing the crystal structure phase stability and electronic structure of FeO_2 using a fully charge self-consistent DFT + DMFT method (see Supplemental Material [18]). Within DFT + DMFT, we perform a full structural optimization of the lattice parameters of the *paramagnetic* HP-PdF_2 phase of FeO_2 and compare our results with experimental data obtained through more precise *in situ* SC-XRD. In Fig. 1 we display our results for the crystal structure parameters obtained by DFT + DMFT. In contrast to the previous DFT + U results [11], we observe that upon compression the O—O distance decreases from 2.286 Å at 17 GPa to 2.085 Å at 70 GPa, which is in close agreement with our SC-XRD data. Indeed, our SC-XRD measurements give ~2.213(7) Å at 36(1) GPa and 2.117(8) Å at 73(2) GPa. Our DFT + DMFT calculations show that at a pressure of ~70 GPa FeO_2 is a poor metal (see Fig. 2) with about 5.21 electrons in the Wannier Fe 3d states (4.07 electrons inside the atomic sphere with radius ~0.78 Å, in accord with a bond valence analysis). Oxygen states are partially occupied with ~0.61 hole states

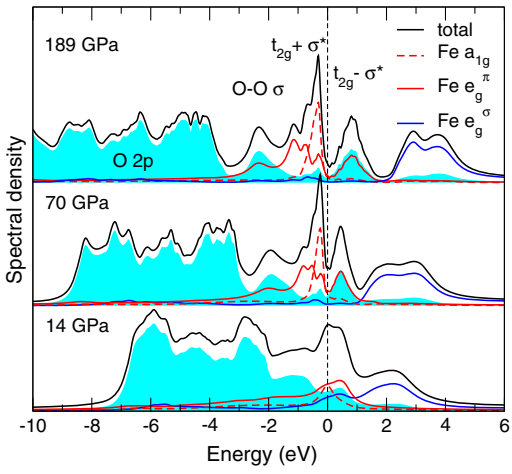

FIG. 2. Fe 3d (a_{1g}, e_g^{π}, and e_g^{σ}) and O 2p (blue shaded area) spectral functions of HP-PdF_2 FeO_2 as obtained by DFT + DMFT for different pressures.

in the Wannier O 2p orbitals. The local magnetic moment is ~1.59 μ_B (fluctuating moment of 0.83 μ_B). Our results for the decomposition of electronic state into atomic configurations (valence states) show that the valence value for Fe is nearly 3+ at ~70 GPa: Fe^{3+} $3d^5$ configuration has a weight of about 50%, with a ~30% admixture of the Fe^{2+} $3d^6$ state ($\sqrt{0.5}|d^5\rangle + \sqrt{0.3}|d^6\rangle$, see Fig. S8 [18]).

In Fig. 2 we see that, due to distorted FeO_6 octahedron symmetry, the Fe t_{2g} states split into a a_{1g} singlet and e_g^{π} doublet. Fe e_g^{σ} orbitals are empty and are located well above the Fermi level at 1–4 eV. Fe t_{2g} states form weakly renormalized ($m/m^* \sim 1.6$) quasiparticle bands near E_F. No evidence for a metal-to-insulator phase transition in FeO_2 (below ~189 GPa) was observed within our fully relaxed DFT + DMFT calculations [11,12], in agreement with experiment. In fact, under experimental setup presented here, samples were black with a metallic shine, implying a metallic state of FeO_2. Moreover, within DFT + DMFT the low-to-high spin-state transition is found to occur below ~14 GPa, i.e., below the stability field of the HP-PdF_2-type FeO_2. Most notably, our DFT + DMFT results confirm that even at ~189 GPa the O—O bond length remains sufficiently large (1.86 Å), implying the absence of covalent "molecular" O—O bonding in FeO_2.

Our DFT + DMFT results agree well with our Mössbauer spectroscopy data that show a low-spin state of nearly 3+ iron ions in the studied pressure range (see below). Most importantly, our fully relaxed and charge self-consistent DFT + DMFT calculations lead to a different bonding picture of FeO_2 in comparison to the analysis by Streltsov *et al.* [14]. Our results reveal the absence of a molecular $(O_2)^{3-}$ bonding state; i.e., in FeO_2 iron has effective charge 3+ and oxygen 1.5−. We see that at ~70 GPa, bonding O—O σ states appear at about −2 eV, while antibonding σ^* states split into the $t_{2g} \pm \sigma^*$ combinations (seen as two peaks at −0.5 and +0.5 eV) due to the mixing with the Fe t_{2g} states at the Fermi level. Importantly, the empty $t_{2g} - \sigma^*$ O—O band is located ~0.5 eV above the Fermi level. We conclude that FeO_2 belongs to the class of negative charge-transfer materials (in which excitation energy for the transfer of electrons from the O 2p to Fe 3d states is negative) [49,50]. In such materials, instead of having an electronic configuration corresponding to the formal valence state, e.g., Fe^{4+} and O^{2-} configuration in FeO_2, the system adopts a configuration with higher occupation of the 3d shell, creating holes on oxygen. At the same time, the bonding-antibonding splitting of the O 2p orbitals is small, just ~2–3 eV, indicating negligible bonding between the two oxygen atoms. This agrees well with our analysis of the charge density distribution in FeO_2 in comparison to magnesium peroxide MgO_2 (space group $Pa\bar{3}$) [51,52]. Our results are summarized in Fig. 3, highlighting the absence of a molecular $(O_2)^{3-}$ or $(O_2)^{2-}$ bonding state in FeO_2 in the studied interval of pressures. In

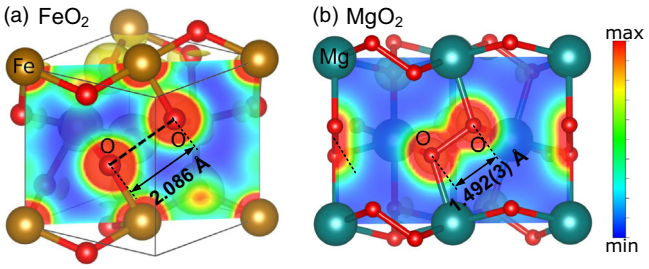

FIG. 3. (a) Crystal structure and valence electron density plot for HP-PdF_2 FeO_2 obtained by DFT + DMFT at ~70 GPa. (b) DFT hybride potential Heyd–Scuseria–Ernzerhof HSE03 results for pyrite-type MgO_2 peroxide at ambient conditions. Max stands for 15% of maximum of charge density $\rho(\mathbf{r})$.

fact, while MgO_2 clearly shows the formation of a molecular $(O_2)^{2-}$ bond with ~21% of a maximal electron density value in the center of the O—O bond, for cubic FeO_2 it is only 5% at 70 GPa (~8% at 189 GPa, see Fig. S8 [18]). Thus, in sharp contrast to MgO_2, no covalent O—O bond is seen for FeO_2. Therefore, the results of explicit examination of the calculated electronic structure and charge density distribution in HP-PdF_2-type FeO_2 confirms our conclusion on the absence of chemical bonding between these oxygen atoms, as well as the fact that the Fe oxidation state is nearly 3+.

Our Mössbauer spectroscopy data (see Fig. S4 [18]) are consistent with iron in the Fe^{3+} state [3,53]. We note that the center shift that we obtained for cubic FeO_2 at 58(2) GPa [0.06(5) mm/s] is in good agreement with that in Ref. [10]. Our experimental and theoretical results thus imply that the oxidation state of oxygen in HP-PdF_2-type FeO_2 is equal to 1.5− due to oxygen-metal negative charge transfer. It is expected to shorten the Fe—O distance and consequently reduce the volume of FeO_6 octahedra, which should cause both iron polyhedra and the entire structure to become highly incompressible. Indeed, fitting the experimental SC-XRD pressure-volume data for cubic FeO_2 with the third-order Birch-Murnaghan equation of state gave a large bulk modulus $K_0 = 305(9)$ GPa ($K' = 4.0$, fixed); the unit cell volume $V_0 = 97.6(3)$ Å^3. The compressibility of FeO_6 octahedra is low [$K_{0,\mathrm{octa}} = 350(4)$ GPa] and the octahedral volume is significantly smaller than that known for any other compound, including those with ferric iron in the low-spin state [Fig. 1(b)].

We complemented studies of cubic FeO_2 by investigations of high-pressure behavior of iron (III) oxyhydroxide, FeO_2H_x. The synthesis of FeO_2H_x was performed by laser heating of a natural single crystal of goethite, α-FeOOH, loaded in Ne as a pressure-transmitting medium to avoid undesirable chemical reactions [54] (see Table S1 [18]). Heating at 1500(100) K and 81(2) GPa resulted in formation of a cubic phase with the lattice parameter $a = 4.430(1)$ Å. The structure was solved and refined from SC-XRD data (Table S2), and the arrangement of Fe and O was found to correspond to the HP-PdF_2-type structure, confirming that FeO_2 and FeO_2H_x are isostructural phases. The lattice parameter suggests the chemical composition $FeO_2H_{0.4}$ [55]. The relatively high value of the shortest O—O distance [~2.262(5) Å] rules out the peroxide-type chemical bonding between oxygen atoms, and the presence of hydrogen does not shorten this bond length.

To confirm the oxidation state of iron in cubic FeO_2H_x, we performed *in situ* x-ray absorption near-edge structure (XANES) measurements on the sample synthesized by laser heating of goethite at 86(2) GPa and 1700(200) K in a DAC equipped with polycrystalline diamond anvils [56]. Powder XRD data confirmed the synthesis of material with the lattice parameter $a = 4.449(5)$ Å (Fig. S5 [18]), which corresponds to the composition $FeO_2H_{0.5}$, while no signs of any unwanted reactions were detected. In the XANES spectra collected in the center of a sample at the Fe K_α edge, the preedge peak narrows after synthesis of $FeO_2H_{0.5}$, and negligible changes in the edge feature are observed; however, the position of the absorption jump remains the same for the starting FeOOH and cubic $FeO_2H_{0.5}$ (Fig. 4), inferring that iron does not alter its oxidation state during this transformation and remains 3+. The results of XANES mapping and comparative contrast maps [57] confirm the high homogeneity of a sample (with traces of FeOOH on the sample's edge, see Fig. S6) and points toward presence of Fe^{3+} atoms in the sample.

Generalizing our observations on cubic HP-PdF_2-structured FeO_2 and FeO_2H_x phases and taking into account that compounds with x up to 1 have been described in the literature, we conclude that, at pressures above ~50 GPa, the oxidation state of oxygen can significantly deviate from 2−. Experimental and theoretical results on cubic FeO_2 and FeO_2H_x phases may be concise in terms of the concept of valence. For our purposes, we accept a definition of the

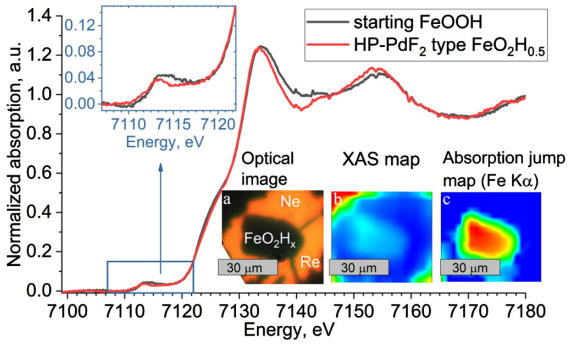

FIG. 4. Normalized x-ray absorption spectra of Fe K_α edge for $FeO_2H_{0.5}$ synthesized at 86(2) GPa and 1700(200) K and starting FeOOH (DAC5, see Table S1). Centroid positions are 7114.54(9) and 7114.76(73) eV, correspondingly. Bottom right insets: (a) Microphotograph of $FeO_2H_{0.5}$ sample; (b),(c) XAS absorption contrast and absorption jump maps of a sample chamber (palette reflects the relative values of the absorption jump).

"valence" of an element as a measure of its combining power with other atoms when it forms chemical compounds or, as in the bond valence model [58], as the number of electrons the atom uses for bonding. Thus, in the HP-PdF_2-type structured FeO_2 and $FeO_2H_{0.5}$ iron has the valence 3+ and oxygen has—1.5 and 1.75, correspondingly. Reducing the oxygen valence from 2, common for oxides, down to 1.5 can be explained by a formation of a localized hole at oxygen sites, which leads to a reduction of the Fe—O distance and, as a consequence, of the volume of FeO_6 octahedra.

In conclusion, using *in situ* SC-XRD, Mössbauer spectroscopy, and XANES in combination with DFT + DMFT, we determine the electronic structure, magnetic and valence states, and phase stability of FeO_2 and FeO_2H_x under pressure. Our results on compressional behavior of FeO_2 obtained by DFT + DMFT are in excellent agreement with SC-XRD data. The structure analysis of FeO_2 reveals the HP-PdF_2-type structure and suggests no chemical bonding between oxygen atoms. We show that in FeO_2, which could be formed above ~45 GPa, i.e., at the conditions corresponding to those in Earth's lower mantle at the depth of ~1150 km, iron is ferric (3+) and oxygen has a formal valence reduced to 1.5−. However, the presence of FeO_2 and FeO_2H_x phases in the lower mantle and at the core-mantle boundary is unlikely, as in these regions the oxygen fugacity necessary for formation of Fe^{3+} [59] is not achieved. Nevertheless, the appearance of oxygen with the low valence can affect the state and properties of various (Fe—O)-bearing mantle minerals that makes accounting of it of great importance for modeling the chemistry of deep Earth's interior.

We acknowledge the Deutsches Elektronen-Synchrotron (DESY, PETRA III), the European Synchrotron Radiation Facility (ESRF), and the Advance Photon Source (APS) for provision of beamtime. N. D. and L. D. thank the Federal Ministry of Education and Research, Germany (BMBF, Grant No. 05K19WC1) and the Deutsche Forschungsgemeinschaft (DFG Projects No. DU 954–11/1, No. DU 393–9/2, and No. DU 393–13/1) for financial support. N. D. and I. A. A. thank the Swedish Government Strategic Research Area in Materials Science on Functional Materials at Linköping University (Faculty Grant SFO-Mat-LiU No. 2009 00971). Electronic structure calculations were supported by the Russian Science Foundation (Project No. 18-12-00492). Theoretical analysis of chemical bonding was supported by the Ministry of Science and Higher Education of the Russian Federation in the framework of Increase Competitiveness Program of NUST "MISIS" (No. K2-2019-001) implemented by a governmental decree, No. 211. Support from the Knut and Alice Wallenberg Foundation (Wallenberg Scholar Grant No. KAW-2018.0194), the Swedish Government Strategic Research Areas and SeRC, and the Swedish Research Council (VR) Grant No. 2019-05600 is gratefully acknowledged.

*Corresponding author.
koemets.e@gmail.com
†Corresponding author.
ivan.v.leonov@yandex.ru

[1] A. B. Woodland, J. Kornprobst, and A. Tabit, Ferric iron in orogenic lherzolite massifs and controls of oxygen fugacity in the upper mantle, Lithos **89**, 222 (2006).
[2] B. Lavina and Y. Meng, Unraveling the complexity of iron oxides at high pressure and temperature: Synthesis of Fe_5O_6, Sci. Adv. **1**, e1400260 (2015).
[3] E. Bykova, L. Dubrovinsky, N. Dubrovinskaia, M. Bykov, C. McCammon, S. V. Ovsyannikov, H.-P. Liermann, I. Kupenko, A. I. Chumakov, R. Ruffer, M. Hanfland, and V. Prakapenka, Structural complexity of simple Fe_2O_3 at high pressures and temperatures, Nat. Commun. **7**, 10661 (2016).
[4] S. V. Ovsyannikov, M. Bykov, E. Bykova, K. Glazyrin, R. S. Manna, A. A. Tsirlin, V. Cerantola, I. Kupenko, A. V. Kurnosov, I. Kantor, A. S. Pakhomova, I. Chuvashova, A. I. Chumakov, R. Rüffer, C. McCammon, and L. S. Dubrovinsky, Pressure tuning of charge ordering in iron oxide, Nat. Commun. **9**, 4142 (2018).
[5] R. Sinmyo, E. Bykova, S. V Ovsyannikov, C. Mccammon, I. Kupenko, L. Ismailova, and L. Dubrovinsky, Discovery of Fe_7O_9: A new iron oxide with a complex monoclinic structure, Sci. Rep. **6**, 32852 (2016).
[6] Q. Hu, D. Y. Kim, W. Yang, L. Yang, Y. Meng, L. Zhang, and H. K. Mao, FeO_2 and FeOOH under deep lower-mantle conditions and Earth's oxygen-hydrogen cycles, Nature (London) **534**, 241 (2016).
[7] Q. Hu and J. Liu, Deep mantle hydrogen in the pyrite-type FeO_2-FeO_2H system, Geosci. Front. **12**, 975 (2020).
[8] M. Nishi, Y. Kuwayama, J. Tsuchiya, and T. Tsuchiya, The Pyrite-type high-pressure form of FeOOH, Nature (London) **547**, 205 (2017).
[9] E. Boulard, M. Harmand, F. Guyot, G. Lelong, G. Morard, D. Cabaret, S. Boccato, A. D. Rosa, R. Briggs, S. Pascarelli, and G. Fiquet, Ferrous iron under oxygen-rich conditions in the deep mantle, Geophys. Res. Lett. **46**, 1348 (2019).
[10] J. Liu, Q. Hu, W. Bi, L. Yang, Y. Xiao, P. Chow, Y. Meng, V. B. Prakapenka, H. K. Mao, and W. L. Mao, Altered chemistry of oxygen and iron under deep earth conditions, Nat. Commun. **10**, 153 (2019).
[11] B. G. Jang, D. Y. Kim, and J. H. Shim, Metal-insulator transition and the role of electron correlation in FeO_2, Phys. Rev. B **95**, 075144 (2017).
[12] B. G. Jang, J. Liu, Q. Hu, K. Haule, H. K. Mao, W. L. Mao, D. Y. Kim, and J. H. Shim, Electronic spin transition in FeO_2: Evidence for Fe(II) with peroxide O_2^{2-}, Phys. Rev. B **100**, 014418 (2019).
[13] E. Bykova, Single-crystal x-ray diffraction at extreme conditions in mineral physics and material sciences, Thesis. Bayreuther Graduiertenschule Für Math. Und Naturwissenschaften, 2015, p. 282.
[14] S. S. Streltsov, A. O. Shorikov, S. L. Skornyakov, A. I. Poteryaev, and D. I. Khomskii, Unexpected 3+ valence

of iron in FeO_2, a geologically important material lying in between oxides and peroxides, Sci. Rep. **7**, 13005 (2017).
[15] A. O. Shorikov and S. V. Streltsov, Equation of state of FeO_2, J. Magn. Magn. Mater. **459**, 280 (2018).
[16] A. T. Garcia-Sosa and M. Castro, Density functional study of FeO_2, FeO_2^+, and FeO_2^-, Int. J. Quantum Chem. **80**, 307 (2000).
[17] C. Lu, M. Amsler, and C. Chen, Unraveling the structure and bonding evolution of the newly discovered iron oxide FeO_2, Phys. Rev. B **98**, 054102 (2018).
[18] See Supplemental Material at http://link.aps.org/supplemental/10.1103/PhysRevLett.126.106001 for additional tables, figures, description of methods, and discussions, which includes Refs. [19–34].
[19] A. R. Kjekshus and T. R. Rakke, Preparations and properties of magnesium, copper, zinc, and xadmium dichalcogenides, Acta Chem. Scand. Ser. A **302**, 080617 (1979).
[20] D. M. Vasiukov, L. Dubrovinsky, I. Kupenko, V. Cerantola, G. Aprilis, L. Ismailova, E. Bykova, C. McCammon, C. Prescher, A. I. Chumakov, and N. Dubrovinskaia, Pressure-induced spin pairing transition of Fe^{3+} in oxygen octahedra, arXiv:1710.03192.
[21] I. Kantor, V. Prakapenka, A. Kantor, P. Dera, A. Kurnosov, S. Sinogeikin, N. Dubrovinskaia, and L. Dubrovinsky, BX90: A new diamond anvil cell design for x-ray diffraction and optical measurements, Rev. Sci. Instrum. **83**, 125102 (2012).
[22] M. Merlini and M. Hanfland, Single-crystal diffraction at megabar conditions by synchrotron radiation, High Press. Res. **33**, 511 (2013).
[23] H. P. Liermann, Z. Konopková, W. Morgenroth, K. Glazyrin, J. Bednarčik, E. E. McBride, S. Petitgirard, J. T. Delitz, M. Wendt, Y. Bican, A. Ehnes, I. Schwark, A. Rothkirch, M. Tischer, J. Heuer, H. Schulte-Schrepping, T. Kracht, and H. Franz, The extreme conditions beamline P02.2 and the extreme conditions science infrastructure at PETRA III, J. Synchrotron Radiat. **22**, 908 (2015).
[24] C. Prescher and V. B. Prakapenka, DIOPTAS: A program for reduction of two-dimensional x-ray diffraction data and data exploration, High Press. Res. **35**, 223 (2015).
[25] C. Prescher, C. McCammon, and L. Dubrovinsky, MossA: A program for analyzing energy-domain Mössbauer spectra from conventional and synchrotron sources, J. Appl. Crystallogr. **45**, 329 (2012).
[26] G. M. Sheldrick, Crystal structure refinement with SHELXL, Acta Crystallogr. Sect. C **71**, 3 (2015).
[27] K. Momma and F. Izumi, VESTA 3 for three-dimensional visualization of crystal, volumetric and morphology data, J. Appl. Crystallogr. **44**, 1272 (2011).
[28] I. Leonov, V. I. Anisimov, and D. Vollhardt, Metal-insulator transition and lattice instability of paramagnetic V_2O_3, Phys. Rev. B **91**, 195115 (2015).
[29] G. Trimarchi, I. Leonov, N. Binggeli, D. Korotin, and V. I. Anisimov, LDA+DMFT implemented with the pseudopotential plane-wave approach, J. Phys. Condens. Matter **20**, 135227 (2008).
[30] E. Gull, A. J. Millis, A. I. Lichtenstein, A. N. Rubtsov, M. Troyer, and P. Werner, Continuous-time Monte Carlo methods for quantum impurity models, Rev. Mod. Phys. **83**, 349 (2011).
[31] G. Kresse and J. Furthmüller, Efficiency of *ab-initio* total energy calculations for metals and semiconductors using a plane-wave basis set, Comput. Mater. Sci. **6**, 15 (1996).
[32] D. Joubert, From ultrasoft pseudopotentials to the projector augmented-wave method, Phys. Rev. B **59**, 1758 (1999).
[33] G. Kresse and J. Furthmüller, Efficient iterative schemes for *ab initio* total-energy calculations using a plane-wave basis set, Phys. Rev. B **54**, 11169 (1996).
[34] J. Heyd, G. E. Scuseria, and M. Ernzerhof, Hybrid functionals based on a screened coulomb potential, J. Chem. Phys. **118**, 8207 (2003).
[35] A. Georges, G. Kotliar, W. Krauth, and M. Rozenberg, Dynamical mean-field theory of strongly correlated fermion systems and the limit of infinite dimensions, Rev. Mod. Phys. **68**, 13 (1996).
[36] L. V. Pourovskii, B. Amadon, S. Biermann, and A. Georges, Self-consistency over the charge density in dynamical mean-field theory: A linear muffin-tin implementation and some physical implications, Phys. Rev. B **76**, 235101 (2007).
[37] I. Leonov, Metal-insulator transition and local-moment collapse in FeO under pressure, Phys. Rev. B **92**, 085142 (2015).
[38] I. Leonov, L. Pourovskii, A. Georges, and I. A. Abrikosov, Magnetic collapse and the behavior of transition metal oxides at high pressure, Phys. Rev. B **94**, 155135 (2016).
[39] E. Greenberg, R. Nazarov, A. Landa, J. Ying, R. Q. Hood, B. Hen, R. Jeanloz, V. B. Prakapenka, V. V. Struzhkin, G. Kh. Rozenberg, and I. Leonov, Phase transitions and spin-state of iron in FeO at the conditions of Earth's deep interior, arXiv:2004.00652.
[40] S. L. Skornyakov, V. I. Anisimov, D. Vollhardt, and I. Leonov, Effect of electron correlations on the electronic structure and phase stability of FeSe upon lattice expansion, Phys. Rev. B **96**, 035137 (2017); Correlation strength, Lifshitz transition, and the emergence of a two-dimensional to three-dimensional crossover in FeSe under pressure, Phys. Rev. B **97**, 115165 (2018).
[41] E. Greenberg, I. Leonov, S. Layek, Z. Konopkova, M. P. Pasternak, L. Dubrovinsky, R. Jeanloz, I. A. Abrikosov, and G. K. Rozenberg, Pressure-Induced Site-Selective Mott Insulator-Metal Transition in Fe_2O_3, Phys. Rev. X **8**, 031059 (2018).
[42] I. Leonov, G. K. Rozenberg, and I. A. Abrikosov, Charge disproportionation and site-selective local magnetic moments in the post-Perovskite-type Fe_2O_3 under ultra-high pressures, npj Comput. Mater. **5**, 90 (2019).
[43] I. Leonov, A. O. Shorikov, V. I. Anisimov, and I. A. Abrikosov, Emergence of quantum critical charge and spin-state fluctuations near the pressure-induced Mott transition in MnO, FeO, CoO, and NiO, Phys. Rev. B **101**, 245144 (2020).
[44] E. Ito, H. Fukui, T. Katsura, D. Yamazaki, T. Yoshino, Y. I. Aizawa, A. Kubo, S. Yokoshi, K. Kawabe, S. Zhai, A. Shatzkiy, M. Okube, A. Nozawa, and K. I. Funakoshi, Determination of high-pressure phase equilibria of Fe_2O_3 using the Kawai-type apparatus equipped with sintered diamond anvils, Am. Mineral. **94**, 205 (2009).

[45] W.-K. Li, G.-D. Zhou, and T. C. W. Mak, *Advanced Structural Inorganic Chemistry* (Oxford University Press, Oxford, 2008), Vol. 10.

[46] Y. Shirako, X. Wang, Y. Tsujimoto, K. Tanaka, Y. Guo, Y. Matsushita, Y. Nemoto, Y. Katsuya, Y. Shi, D. Mori, H. Kojitani, K. Yamaura, Y. Inaguma, and M. Akaogi, Synthesis, crystal structure, and electronic properties of high-pressure PdF_2 type oxides MO_2 (M = Ru, Rh, Os, Ir, Pt), Inorg. Chem. **53**, 11616 (2014).

[47] J. Haines, J. M. Leger, M. W. Schmidt, J. P. Petitet, a S. Pereira, J. a H. Da Jornada, and S. Hull, Structural characterization of the $Pa\bar{3}$-type, high pressure phase of ruthenium dioxide, J. Phys. Chem. Solids **59**, 239 (1998).

[48] C. T. Prewitt and R. T. Downs, High-pressure crystal chemistry, Rev. Mineral. **37**, 284 (1998).

[49] J. Zaanen, G. A. Sawatzky, and J. W. Allen, Band Gaps and Electronic Structure of Transition-Metal Compounds, Phys. Rev. Lett. **55**, 418 (1985).

[50] M. A. Korotin, V. I. Anisimov, D. I. Khomskii, and G. A. Sawatzky, CrO_2: A Self-Doped Double Exchange Ferromagnet, Phys. Rev. Lett. **80**, 4305 (1998).

[51] Q. Zhu, A. R. Oganov, and A. O. Lyakhova, Novel stable compounds in the Mg–O system under high pressure, Phys. Chem. Chem. Phys. **15**, 7696 (2013).

[52] S. S. Lobanov, Q. Zhu, N. Holtgrewe, C. Prescher, V. B. Prakapenka, A. R. Oganov, and A. F. Goncharov, Stable magnesium peroxide at high pressure, Sci. Rep. **5**, 13582 (2015).

[53] P. Gütlich, E. Bill, and A. X. Trautwein, Mössbauer Spectroscopy and Transition Metal Chemistry: Fundamentals and Applications (Springer Science & Business Media, 2010).

[54] E. Koemets, L. Yuan, E. Bykova, K. Glazyrin, E. Ohtani, and L. Dubrovinsky, Interaction between FeOOH and NaCl at extreme conditions: Synthesis of novel $Na_2FeCl_4OH_x$ compound, Minerals **10**, 51 (2020).

[55] Q. Hu, D. Y. Kim, J. Liu, Y. Meng, L. Yang, D. Zhang, W. L. Mao, and H. Mao, Dehydrogenation of goethite in Earth's deep lower mantle, Proc. Natl. Acad. Sci. U.S.A. **114**, 1498–1501 (2017).

[56] N. Ishimatsu, K. Matsumoto, H. Maruyama, N. Kawamura, M. Mizumaki, H. Sumiya, and T. Irifune, Glitch-free x-ray absorption spectrum under high pressure obtained using nano-polycrystalline diamond anvils, J. Synchrotron Radiat. **19**, 768 (2012).

[57] G. Aprilis, I. Kantor, I. Kupenko, V. Cerantola, A. Pakhomova, I. E. Collings, R. Torchio, T. Fedotenko, S. Chariton, M. Bykov, E. Bykova, E. Koemets, D. M. Vasiukov, C. McCammon, L. Dubrovinsky, and N. Dubrovinskaia, Comparative study of the influence of pulsed and continuous wave laser heating on the mobilization of carbon and its chemical reaction with iron in a diamond anvil cell, J. Appl. Phys. **125**, 095901 (2019).

[58] *Bond Valences*, edited by I. D. Brown and K. R. Poeppelmeier (Springer Berlin Heidelberg, Berlin, 2014).

[59] D. J. Frost and C. A. McCammon, The redox state of Earth's mantle, Annu. Rev. Earth Planet Sci. **36**, 389 (2008).